In Situ Iridium L_{III}-Edge X-ray Absorption and Surface Enhanced Raman Spectroscopy of Electrodeposited Iridium Oxide Films in Aqueous Electrolytes

Yibo Mo,[†] Ionel C. Stefan,[†] Wen-Bin Cai,[†] Jian Dong,[‡] Paul Carey,[‡] and Daniel A. Scherson*[,†]

Departments of Chemistry and Biochemistry, Case Western Reserve University, Cleveland, Ohio 44106

Received: December 10, 2001

Structural and electronic aspects of IrO_2 films prepared by electrodeposition on Au substrates were investigated by in situ L_{III}-edge X-ray absorption and surface enhanced Raman spectroscopies in both acid and alkaline aqueous solutions. Linear correlations were found between the extent of oxidation of Ir^{3+} in the films determined from a statistical fit of the white line, which includes contributions from each of the sites differing by a single electron, and from coulometric analysis of the voltammetric curves. Analysis of the extended X-ray absorption fine structure (EXAFS) yielded Ir−O bond lengths decreasing in the sequence 2.02, 1.97, and 1.93 Å for Ir^{3+}, Ir^{4+}, and Ir^{5+} sites, respectively. Whereas SERS provided evidence for the presence of crystalline IrO_2 in the highly hydrated films, the lack of intense shells in the Fourier transform of the EXAFS function beyond the nearest oxygen neighbors indicates that the films do not display long-range order.

Introduction

Iridium oxide films (IROF) display interesting electrochemical characteristics with applications ranging from electrocatalysis[1−5] and electrochromism[6−9] to sensors[10−13] and supercapacitors.[14] Attention in recent years has centered on the use of this material in neural stimulation and recording electrodes[15−17] to fully exploit its high charge storage capabilities, high rates of charge/discharge, and ease of miniaturization. Such unique properties provide means for fast charge injection, thereby reducing faradaic generation of harmful species, e.g., radicals, in the vicinity of neural or other tissue.[18] Despite years of research, no consensus has been reached regarding the factors that control the performance of IROF electrodes. Much of the controversy stems from differences in the way specimens are prepared, which include such diverse methods as sputtering, electrochemical oxidation or deposition, and thermal oxidation of pure metal films.[19,20] In particular, sputtered iridium oxide films (SIROF) grown either by oxidative (reactive) sputtering or by thermal oxidation of sputtered Ir metal films are generally dense,[21,22] ca. 10 g/cm^3 compared to 11.7 g/cm^3 for anhydrous IrO_2, and exhibit voltammetric curves in acid media characterized by broad, poorly defined peaks.[21,23] On the basis of in situ Ir L_{III}-edge X-ray absorption spectroscopy (XAS) and impedance spectroscopy studies in 1 M H_2SO_4 solutions, Pauporte and co-workers identified only a single redox process in the potential range −0.2 to 1.1 V vs SCE ascribed to the Ir^{3+}/Ir^{4+} oxide couple.[23]

Electrochemical oxidation of sputtered metallic Ir yields anodic films (AIROF) with highly porous and hydrated structure and significantly lower densities than SIROF, ca. 2 g/cm^3, and much better defined voltammetric peaks in both acid and basic solutions.[24] Huppauff and Lengeler studied AIROF in 1 N H_2SO_4 solutions by in situ Ir L_{III}-edge XAS and concluded that in the potential range 0−1.2 V vs Ag/AgCl the oxidation state of Ir sites varies from 3+ to 4.8+.[25]

In contrast to SIROF and AIROF, which contain variable amounts of Ir metal, highly porous hydrated IrO_2 films produced by electrodeposition (EIROF) appear to incorporate only electrochemically active Ir sites and, as such, are especially suited for fundamental quantitative studies.[20] Although EIROF are receiving increased attention from a technological viewpoint, no information regarding their structural and vibrational properties appears to be available.

This work presents a combined in situ Ir L_{III}-edge XAS and surface enhanced Raman spectroscopy (SERS) study of EIROF electrodes electrodeposited on either smooth or roughened gold electrodes in alkaline (0.3 M Na_2CO_3) and, to a lesser extent, acid (0.5 N H_2SO_4) solutions. As will be shown, the particularly well-defined voltammetric behavior of EIROF in the basic electrolyte made it possible to correlate quantitatively the white line behavior with the state of charge of the film, and, hence, assign each of the redox features to distinct electron-transfer processes. This information is of special significance as it enables direct links to be established between vibrational and structural properties, e.g., Ir−O average bond distance, and oxidation states.

Experimental Section

Iridium oxide electrodes of the EIROF type supported on either Au-coated Melinex sheets (for XAS) or roughened solid Au electrodes (for SERS) were prepared by electrodeposition following the method described in ref 20, yielding voltammetric curves in acid and base in excellent agreement with those reported in the literature (see upper panels, Figure 1).[15,20,26]

In situ XAS spectra were acquired at beamline 4-3 at the Stanford Synchrotron Radiation Laboratory (SSRL) operating at ring currents in the range 50−100 mA. A set of Si(220) crystals was used to monochromatize the beam. X-ray absorption spectra over the X-ray absorption near edge structure (XANES) and extended X-ray absorption fine structure (EXAFS) regions were collected in the fluorescence mode with the electrode placed at an angle of 45° with respect to a 13-element Ge detector. The Ir L_{III}-edge energy, i.e., 11 215 eV, was calibrated

* Corresponding author. Telephone: 216-368-5186. Fax: 216-368-3006. E-mail: dxs16@po.cwru.edu.
[†] Department of Chemistry.
[‡] Department of Biochemistry.

10.1021/jp014452p CCC: $22.00
Published on Web 03/14/2002

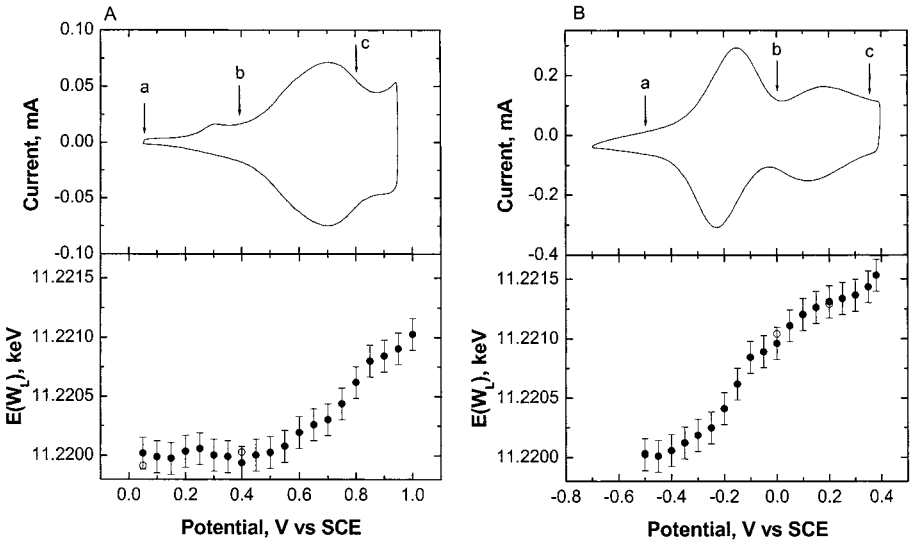

Figure 1. Upper panels: Cyclic voltammograms of EIROF deposited on Au-coated Melinex in 0.5 M H_2SO_4 (panel A) and 0.3 M Na_2CO_3 aqueous solutions (panel B) used for in situ XAS measurements. Lower panels: Plot of the white line peak position, $E(W_L)$, as a function of potential based on the analysis of the XANES (see text for details).The empty symbols in these figures were collected in independent experiments.

using the first inflection point of the edge region of a metallic Ir foil recorded in transmission after each fill.

For the analysis of the edge region the X-ray energy was scanned in the range −50 to −20 eV in increments $\Delta E = 2$ eV and −20 to +20 eV ($\Delta E = 0.35$ eV) with respect to Ir L_{III} edge, and in steps of 0.5 $Å^{-1}$ thereafter up to 13 $Å^{-1}$, i.e., just below the onset of the Au L_{III} edge (11 918 eV), to allow a more reliable preedge correction and background normalization. Spectral decomposition of the white line was obtained using the LC XANES routine of WinXAS,[27] which relies on statistical fitting methods and spectral additivity to determine the composition of a mixture, e.g., A + B, using as input the white lines of A and B, i.e., its pure constituent materials. This allows, in our case, the extent of conversion of, for example, Ir^{x+} into Ir^{y+}, as the redox reaction progresses, provided $|x - y| = 1$, where x is 3 and 4, and y is 4 and 5, to be determined spectroscopically and the results then compared to those derived from a coulometric analysis. It will prove convenient, however, to represent sequential one-electron events as a continuous process by using an arbitrary redox state, e.g., Ir^{3+} for the system under study, as an initial reference. On this basis, values larger than 1 indicate films in which the oxidation state of Ir sites is larger than 4+.

For EXAFS, the X-ray energy was scanned with respect to Ir L_{III} edge in the range −100 to −20 eV ($\Delta E = 2$ eV) and −20 to +20 eV ($\Delta E = 0.35$ eV) and in steps of 0.05 $Å^{-1}$ up to 13 $Å^{-1}$, thereafter (see above). The EXAFS analysis was performed in k-space on the k^3-weighted reduced EXAFS data, $k^3\chi(k)$ vs k, using WinXAS, and single-scattering theoretical phase and amplitude data calculated from FEFF (version 8.1).

Raman spectra were obtained using 647.1 nm laser excitation from an Innova 400 krypton laser system (Coherent) and a back-illuminated CCD detector (Model 1024 EHRB/1, Princeton Instruments) operating at 183 K using a Raman microscope (Kaiser Optical Systems) equipped with a 10× long working-length objective (2.00 cm). Raman activation of the Au substrate prior to film deposition was performed following the method of Weaver et al.[28] In situ Ir L_{III}-edge XAS and SERS measurements of EIROF were performed in both alkaline (ca. 0.3 M Na_2CO_3) and acid (ca. 0.5 M H_2SO_4) aqueous solutions.

Results and Discussion

Electrochemistry. The cyclic voltammograms of EIROF in 0.5 M H_2SO_4 and 0.3 M Na_2CO_3 aqueous solutions electrodeposited on Au electrodes displayed either a single broad peak or two well-defined features assigned formally to Ir^{3+}/Ir^{4+} (acid) and Ir^{3+}/Ir^{4+} and Ir^{4+}/Ir^{5+} (alkaline) redox processes, as shown in the upper panels of Figure 1 for Au-coated Melinex substrates used for in situ XAS measurements (see below). The voltammograms obtained in acid for this type of substrate were found to be tilted toward higher currents at higher potentials owing most likely to IR effects due to the thinness of the Au film. Account for such contributions was made by subtracting a straight line from the entire curve to yield the results shown in Figure 1A. Films polarized at potentials higher than 0.9 V in acid were found to degrade over time; hence, no reliable spectroscopic data could be obtained beyond that limit. The peak at about 0.3 V observed in acid media during the scan in the positive direction has also been found for AIROF by other authors, but its origin still remains unexplained.[25,29]

As clearly indicated, the oxidation of films in basic media is shifted toward more negative potentials allowing a complete second redox feature to be observed prior to the onset of oxygen evolution.

XANES. Figure 2 shows in situ Ir L_{III}-edge XANES in the acid (panel A) and the basic (panel B) solutions recorded in sequence (a, b, c) at the potentials specified by the arrows in the upper panels in Figure 1. The position of the prominent white line, $E(W_L)$, in the acid media remained virtually unchanged for potentials in the range $0.05 < E < 0.40$ V, i.e., prior to the onset of the main voltammetric peak. As indicated, however, both the intensity and width of this line increased as the films were oxidized for acid and basic solutions.

Insight into these effects was gained from a more detailed series of experiments in which the XANES was measured every 50 mV during a scan in the positive direction. The results indicated a monotonic variation of the white line peak position, $E(W_L)$, as a function of potential (see lower panels in Figure 1A and 1B, for acid and alkaline media, respectively). The empty symbols in this plot were collected in independent experiments and illustrate the high degree of reproducibility of these measurements. As evidenced from the data in the acid

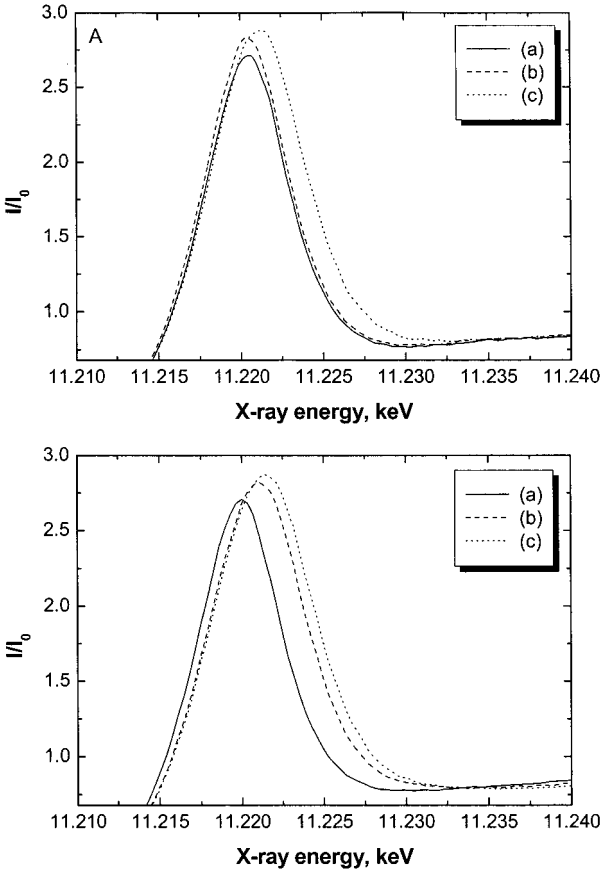

Figure 2. In situ Ir L_{III}-edge XANES in acid (panel A) and basic (panel B) solutions recorded in sequence (a, b, c) at the potentials specified by the arrows in the upper panels in Figure 1.

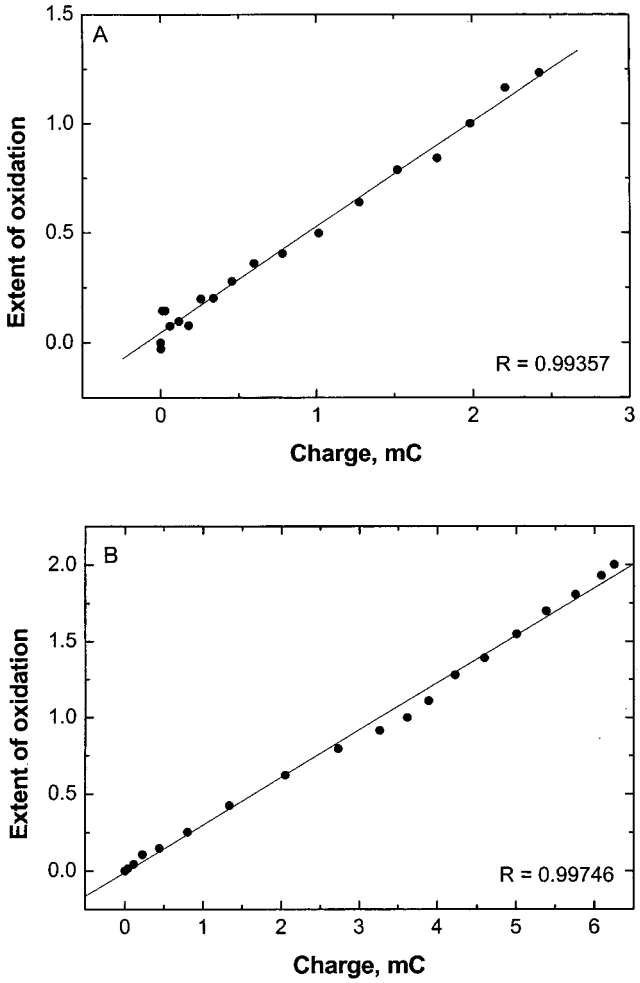

Figure 3. Extent of oxidation based on LCXANES analysis versus charge calculated by coulometry from the voltammetric curves, for data collected in acid (panel A) and basic media (panel B).

solution, the voltammetric peak at ca. 0.3 V is not accompanied by discernible shifts in $E(W_L)$ and hence may not be related to changes in oxidation state. Furthermore, for potentials larger than 0.5 V in acid and larger than −0.4 V in base, $E(W_L)$ was found to shift monotonically toward higher energies. In fact, the absolute values of $E(W_L)$ at the most negative potentials for both media were the same, i.e., 12 200 eV, and the total shift in $E(W_L)$ over the range which embraces the more negative redox process (0.5 to 0.9 V in acid and −0.4 to 0.0 V in base), were also equal, ca. 1 eV. This observation provides clear evidence that the Ir sites involved are indeed the same, as will be further supported by the EXAFS analysis below.

An additional total shift in $E(W_L)$ of about 0.5 eV was observed after scanning the potential over the second redox peak in the basic media consistent with the further oxidation of Ir sites in the film to yield formally Ir^{5+}. It becomes evident from the data in the lower panel in Figure 1 that the correlation between $E(W_L)$ and potential is not linear. In earlier in situ Ir L_{III}-edge XAS studies, Huppauff and Lengeler used $E(W_L)$ values for Ir oxalate and Ir oxide as standards for Ir^{3+} and Ir^{4+}, to estimate, based on a linear extrapolation, oxidation states for Ir in AIROF films in 1 N H_2SO_4 beyond 4+.[25] Based on this model, these authors concluded that at the most positive potentials examined, i.e., 1.2 vs Ag/AgCl, the oxidation state of Ir reached a value of 4.8+. More recently, however, Pauporte et al. failed to obtain evidence for the presence of Ir sites in an oxidation state larger than 4+ for SIROF in the same media over a very similar potential range.[23] No data appear to be available for EIROF.

The well-defined voltammetric behavior observed in the basic electrolyte allows more rigorous correlations to be drawn between $E(W_L)$ and the state of charge of the film without relying on extrapolations. As demonstrated by Petit et al.,[20] all Ir sites in EIROF are electrochemically active, allowing a highly reliable and quantitative coulometric/spectroscopic analysis; i.e., the spectral response does not contain contributions from inactive Ir species. This factor is key to the analysis to follow.

From a general perspective, the white line contains contributions due to all Ir sites present in the film in their various redox states, and the extent of such contributions is proportional to the number of each of such Ir sites. Hence, if the spectral features of Ir sites in their single redox states are known, it becomes possible to decompose the white line of mixtures of two states into its constituents. On the basis of this approach and using the LC XANES routine of WinXAFS (see Experimental Section), the fraction of sites in each of two oxidation states was determined. Strong support for the validity of this method was obtained from plots of the spectroscopically derived fraction of sites versus that calculated by coulometry from the voltammetric curves, which yielded remarkable linear behavior ($R > 0.99$) for data collected in both acid and basic media (Figure 3).

EXAFS. Figure 4 shows the $k^3\chi(k)$ vs k (upper panels) and the corresponding Fourier transforms (lower panel) for data collected in acid (panel A) and basic media (panel B) at the potentials indicated by arrows in panels A and B of Figure 1, respectively. The dotted lines represent experimental data and the solid lines the best fits obtained from a statistical analysis

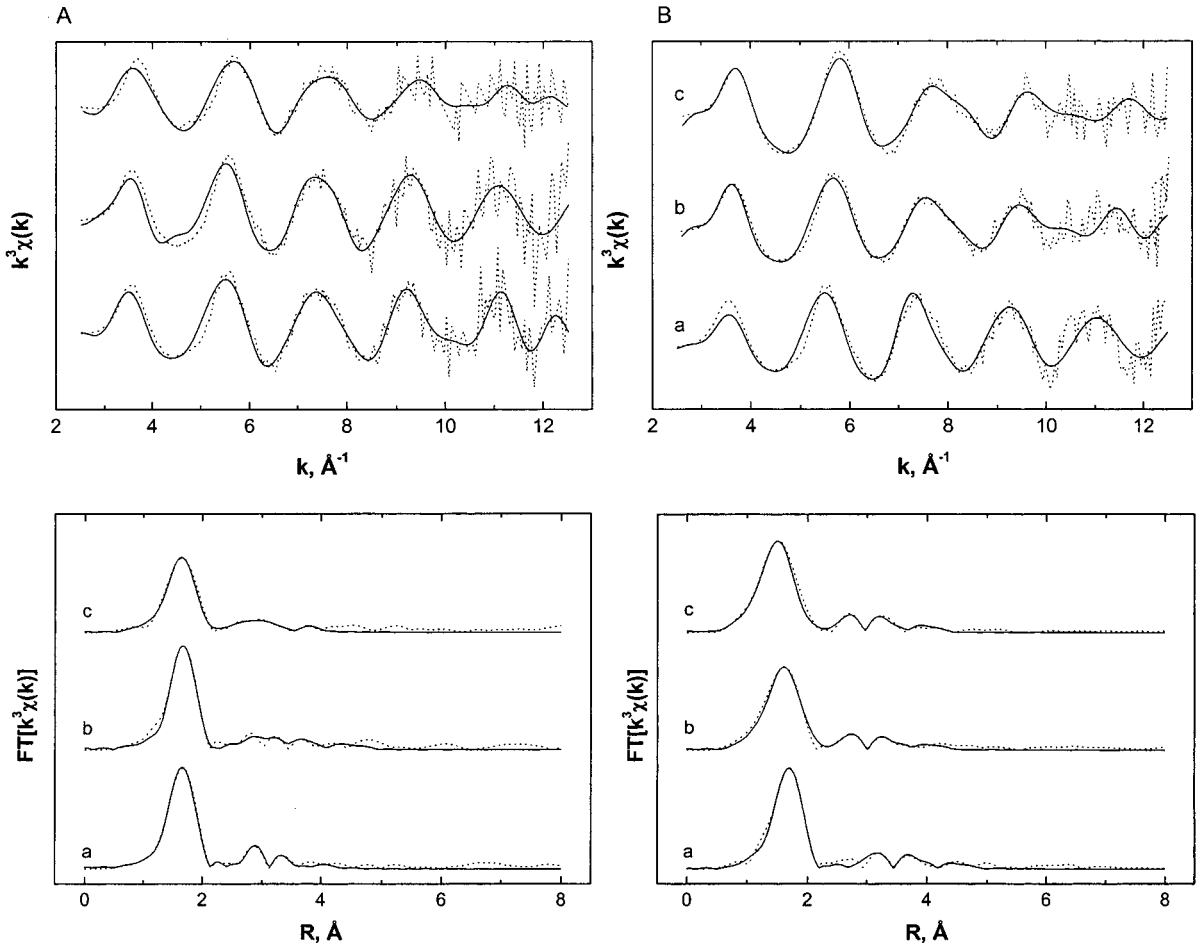

Figure 4. Plots of $k^3\chi(k)$ vs k (upper panels) and corresponding Fourier transforms (lower panels) for data collected in acid (A) and basic media (B) at the potentials indicated by arrows in panels A and B, respectively, of Figure 1. The solid lines are best fits obtained from a statistical analysis of the EXAFS data based on theoretical phases and amplitudes for the first oxygen shell and two single scattering Ir shells of IrO_2.

TABLE 1: Structural Parameters for EIROF Electrodes Derived from the Analysis of in Situ EXAFS Data[a]

solution	potential, V	d(IrO), Å	σ^2, Å^2	ΔE_0
0.5 M H_2SO_4	0.05	2.02(6)	0.004(2)	3.98
	0.37	2.02(4)	0.003(5)	3.86
	0.80	1.97(5)	0.012(9)	3.78
0.3 M Na_2CO_3	−0.50	2.02(9)	0.005(2)	3.92
	−0.05	1.97(6)	0.009(4)	3.85
	0.37	1.93(7)	0.011(1)	3.88

[a] An average of five scans at each applied potential was used for the EXAFS analysis. The background was extracted using seven spline sections of cubic-weighted data from 1 to 12.5 Å^{-1} and then sectioned from 2.5 to 12.5 Å^{-1} for curve fitting with single scattering phases and amplitudes for one Ir−O and two Ir−Ir shells calculated by FEFF8.1. The scale factor was varied from 0.35 to 0.87 while maintaining N fixed at 6 for the nearest Ir−O shell.

of the EXAFS data based on single scattering[30] theoretical phases and amplitudes for the first oxygen shell and two Ir shells of IrO_2 (rutile structure).[31] Numerical values for all fitting parameters for the Ir−O shell at all measured potentials are given in Table 1. Several interesting conclusions can be drawn from these data:

1. The films at 0.8 V in acid and −0.05 V vs SCE in base are best represented as IrO_2, for which the average Ir−O distance d(Ir−O) based on X-ray diffraction is 1.98 Å, i.e., two bonds with d(Ir−O) 1.959 Å and four bonds with d(Ir−O) 1.995 Å to form a distorted octahedron. In fact, an EXAFS analysis of crystalline IrO_2 ex situ yielded 1.98 Å in excellent agreement with the in situ data obtained in the present work.[25]

2. A full one-electron reduction of IrO_2 leads to an increase in d(Ir−O), from 1.97 to 2.02 Å, regardless of the media.

3. The rather high values of the Debye−Waller factors, σ^2, are consistent with the expected structural disorder and hydrated nature of the films. The increase in σ^2 observed upon oxidation is similar to that reported for AIROFs,[25] but not for SIROFs.[23]

4. For acid solutions, d(Ir−O) was found to be virtually identical at both 0.05 and 0.37 V; hence, as the XANES data also suggested, the peak at about 0.3 V does not involve a change the oxidation state of the Ir sites.

5. In alkaline media, d(Ir−O) decreases further upon a full second oxidation step from 1.97 to 1.93 Å, in line with a formal oxidation of sites in the films of 5+.

Raman. Figure 5 shows the SERS spectra of EIROF films supported on roughened Au at different potentials in 0.5 M H_2SO_4 (panel A) and 0.3 M Na_2CO_3 (panel B). Despite differences in their relative intensities, EIROF films at 0.85 V in acid and 0.0 V in base, i.e., in the Ir^{4+} state, displayed a series of peaks at about the same energies, i.e., 744, 620, and a broad band at ca. 500 cm^{-1}. The first of these bands has also been observed for SIROF films on fused silica[32] and assigned to a combination of the A_{1g} and B_{2g} phonon modes, which are particularly prominent in crystalline IrO_2.[33] This band disappears upon either reduction (acid and basic media) or oxidation (basic media), indicative of a loss in long-range order brought about by the redox processes. Unfortunately, no chemical methods have yet been devised for preparing genuine specimens of both the

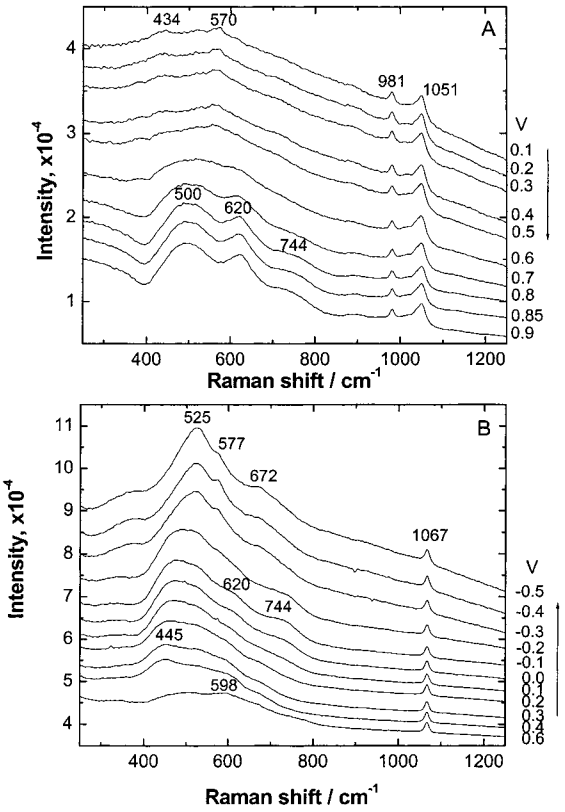

Figure 5. SERS spectra of EIROF films supported on roughened Au at different potentials in 0.5 M H_2SO_4 (panel A) and 0.3 M Na_2CO_3 (panel B) (see text for details).

reduced and oxidized forms of IrO_2, a factor that has hampered their structural and electronic characterization.

Inspection of the spectral data reveals an overall shift of the peaks at ca. 620 and 500 cm^{-1} toward lower energies as the Ir^{4+} films are reduced (see panels A and B) and toward higher energies as the films are oxidized (see panel B). This behavior is consistent with that expected for the Ir−O stretching mode; i.e., the bond length decreases (shift toward higher wavenumbers) or increases (shift toward lower wavenumbers), depending on whether the Ir^{4+} site is oxidized or reduced, as the in situ EXAFS data show (see previous section). Evidence in support of this assignment is provided by the work of Wachs et al.,[34] who established a mathematical correlation between bond length and stretching frequencies for W−O bonds based on experimental data for numerous chemical compounds. According to these authors the bond length, $d(W-O) = R$, and stretching frequency ν (cm^{-1}) are related by an exponential function of the form $\nu = 25823 \exp(-1.902R)$. If this expression is also assumed to apply for Ir−O, the expected ν for $d(Ir-O) = 1.98$ Å would be ca. 600 cm^{-1}, which is not far from that observed experimentally. Moreover, the difference in the magnitude of ν induced by a change in d(Ir−O) of ca. 0.05 Å would amount to 50 cm^{-1}, which again is in fair agreement with the data although the peak is not very well resolved for the Ir^{5+} species (see Figure 5B).

Also noteworthy is the work of Weaver and co-workers,[35] who found a band at 530−570 cm^{-1} in the SERS of ultrathin (3−5 monolayers) AIROF supported on Au in 0.1 M $HClO_4$. Based on their careful studies involving solvent deuteration, these authors assigned the observed feature to an Ir−OH stretching mode; however, their films did not produce monotonic shifts as a function of potential of the type found in this work. Such differences in behavior may well be related to differences in the structure of IrO_2 for such ultrathin films compared to thicker counterparts such as those studied in this work as well as the way in which the films were prepared.

Although somewhat speculative, the band in the 430−500 cm^{-1} range, involving possibly more than one mode, can be tentatively assigned to a O−Ir−O bending mode which would also shift toward lower energies after reduction.

Conclusions

The present work exploits the complementary character of information derived from X-ray absorption and Raman spectroscopies to elucidate structural and electronic aspects of metal oxide films in electrochemical environments, allowing correlations to be drawn between bond distances and stretching frequencies. In addition, it underscores the advantages of electrochemical methods for the synthesis and characterization of materials difficult to obtain by regular chemical means in highly pure form, such as Ir^{3+} and Ir^{5+} oxides as illustrated herein. Overall, the EIROF specimens of the type examined were found to exhibit very well defined redox peaks in the voltammograms and supercapacitive behavior comparable to those of AIROF and vastly superior to those of SIROF. Comparison with the results of a rather recent study[36,37] involving similar electrochemically prepared films of RuO_2 strongly suggest that the lack of long order is a necessary, although not sufficient condition, to confer these oxide materials supercapacitive properties.

Acknowledgment. This work was carried out at the Stanford Synchrotron Radiation Laboratory, which is supported by the U.S. Department of Energy, Division of Material Sciences and Division of Chemical Sciences. Financial support from a grant from DOE-BES is gratefully acknowledged.

References and Notes

(1) Gottesfeld, S.; Srinivasan, S. *J. Electroanal. Chem.* **1978**, *86*, 89.
(2) Rolewicz, J.; Comninellis, C.; Plattner, E.; Hinden, J. *Electrochim. Acta* **1988**, *33*, 573.
(3) Mozota, J.; Conway, B. E. *J. Electrochem. Soc.* **1981**, *128*, 2142.
(4) Hackwood, S.; Schiavone, L. M.; Dautremontsmith, W. C.; Beni, G. *J. Electrochem. Soc.* **1981**, *128*, 2569.
(5) Foti, G.; Gandini, D.; Comninellis, C.; Perret, A.; Haenni, W. *Electrochem. Solid State Lett.* **1999**, *2*, 228.
(6) Dautremontsmith, W. C. *Displays* **1982**, *3*, 67.
(7) Gottesfeld, S.; McIntyre, J. D. E. *J. Electrochem. Soc.* **1979**, *126*, 742.
(8) Sato, Y.; Yanagida, M.; Yamanaka, H.; Tanigawa, H. *J. Electrochem. Soc.* **1989**, *136*, 863.
(9) Mcintyre, J. D. E.; Peck, W. F.; Nakahara, S. *J. Electrochem. Soc.* **1980**, *127*, 1264.
(10) Katsube, T.; Lauks, I.; Zemel, J. N. *Sens. Actuators, B—Phys.* **1982**, *2*, 399.
(11) Burke, L. D.; Mulcahy, J. K.; Whelan, D. P. *J. Electroanal. Chem.* **1984**, *163*, 117.
(12) Hitchman, M. L.; Ramanathan, S. *Anal. Chim. Acta* **1992**, *263*, 53.
(13) Pasztor, K.; Sekiguchi, A.; Shimo, N.; Kitamura, N.; Masuhara, H. *Sens. Actuators, B—Chem.* **1993**, *12*, 225.
(14) Oxley, J. E. In *Proceedings of the 34th International Power Sources Symposium*; Institute of Electrical and Electronics Engineers: New York, 1990; p 346.
(15) Meyer, R. D.; Cogan, S. E.; Nguyen, T. H.; Rauh, R. D. *IEEE Trans. Neural Syst. Rehabil. Eng.* **2001**, *9*, 2.
(16) Weiland, J. D.; Anderson, D. J. *IEEE Trans. Biomed. Eng.* **2000**, *47*, 911.
(17) Blau, A.; Ziegler, C.; Heyer, M.; Endres, F.; Schwitzgebel, G.; Matthies, T.; Stieglitz, T.; Meyer, J. U.; Gopel, W. *Biosens. Bioelectron.* **1997**, *12*, 883.
(18) Stefan, I. C.; Tolmachev, Y. V.; Scherson, D. A. *Anal. Chem.* **2001**, *73*, 527.
(19) Bestaoui, N.; Prouzet, E. *Chem. Mater.* **1997**, *9*, 1036.
(20) Petit, M. A.; Plichon, V. *J. Electroanal. Chem.* **1998**, *444*, 247.
(21) Pauporte, T.; Durand, R. *J. Appl. Electrochem.* **1999**, *30*, 35.

(22) Hackwood, S.; Beni, G.; Gallagher, P. K. *Solid State Ionics* **1981**, *2*, 297.
(23) Pauporte, T.; Aberdam, D.; Hazemann, J. L.; Faure, R.; Durand, R. *J. Electroanal. Chem.* **1999**, *465*, 88.
(24) Pickup, P. G.; Birss, V. I. *J. Electrochem. Soc.* **1988**, *135*, 126.
(25) Huppauff, M.; Lengeler, B. *J. Electrochem. Soc.* **1993**, *140*, 598.
(26) Yamanaka, K. *Jpn. J. Appl. Phys., Part 1—Regul. Pap. Short Notes Rev. Pap.* **1989**, *28*, 632.
(27) Ressler, T. *J. Phys. IV* **1997**, *7*, 269.
(28) Gao, P.; Gosztola, D.; Leung, L. W. H.; Weaver, M. J. *J. Electroanal. Chem.* **1987**, *233*, 211.
(29) Pickup, P. G.; Birss, V. I. *J. Electroanal. Chem.* **1987**, *220*, 83.
(30) Prouzet, E. *J. Phys.: Condens. Matter* **1995**, *7*, 8027.
(31) Bestaoui, N.; Prouzet, E.; Deniard, P.; Brec, R. *Thin Solid Films* **1993**, *235*, 35.
(32) Liao, P. C.; Chen, C. S.; Ho, W. S.; Huang, Y. S.; Tiong, K. K. *Thin Solid Films* **1997**, *301*, 7.
(33) Huang, Y. S.; Lin, S. S.; Huang, C. R.; Lee, M. C.; Dann, T. E.; Chien, F. Z. *Solid State Commun.* **1989**, *70*, 517.
(34) Hardcastle, F. D.; Wachs, I. E. *J. Raman Spectrosc.* **1995**, *26*, 397.
(35) Zou, S. Z.; Chan, H. Y. H.; Williams, C. T.; Weaver, M. J. *Langmuir* **2000**, *16*, 754.
(36) Mo, Y. B.; Antonio, M. R.; Scherson, D. A. *J. Phys. Chem. B* **2000**, *104*, 9777.
(37) Mo, Y. B.; Cai, W. B.; Dong, J. A.; Carey, P. R.; Scherson, D. A. *Electrochem. Solid State Lett.* **2001**, *4*, E37.